crystals

MDPI

Article

Electron Energies of Two-Dimensional Lithium with the Dirac Equation

Raúl García-Llamas [1], Jesús D. Valenzuela-Sau [1,*], Jorge A. Gaspar-Armenta [1] and Rafael A. Méndez-Sánchez [2]

[1] Departamento de Investigación en Física, Universidad de Sonora, Apdo. Postal 5-88, Hermosillo 83000, Sonora, Mexico; raul.llamas@unison.mx (R.G.-L.); jorge.gaspar@unison.mx (J.A.G.-A.)
[2] Instituto de Ciencias Físicas, Universidad Nacional Autónoma de México, Apdo, Postal 48-3, Cuernavaca 62210, Morelos, Mexico; mendez@icf.unam.mx
* Correspondence: daniel.valenzuela@unison.mx

Abstract

The electronic band structure of two-dimensional lithium is calculated using the Dirac equation. Lithium is modeled as a two-dimensional square lattice in which the two strongly bound inner electrons and the fixed nucleus are treated as a positively charged ion (+e), while the outer electron is assumed to be uniformly distributed within the cell. The electronic potential is obtained by considering Coulomb-type interactions between the charges inside the unit cell and those in the surrounding cells. A numerical method that divides the unit cell into small pieces is employed to calculate the potential and then the Fourier coefficients are obtained. The Bloch method is used to determine the energy bands, leading to an eigenvalue matrix equation (in momentum space) of infinite dimension, which is truncated and solved using standard matrix diagonalization techniques. Convergence is analyzed with respect to the key parameters influencing the calculation: the lattice period, the dimension of the eigenvalue matrix, the unit-cell partition used to compute the potential's Fourier coefficients, and the number of neighboring cells that contribute to the electronic interaction.

Keywords: lithium; Dirac equation; electronic band structure; Coulomb potential

Check for updates

Academic Editor: Artem Pronin

Received: 18 October 2025
Revised: 10 December 2025
Accepted: 11 December 2025
Published: 23 January 2026

Copyright: © 2026 by the authors. Licensee MDPI, Basel, Switzerland. This article is an open access article distributed under the terms and conditions of the Creative Commons Attribution (CC BY) license.

1. Introduction

A theoretical study from 1947 predicted that a honeycomb lattice of carbon atoms would exhibit a zero-gap band structure due to weak interlayer interactions [1]. In that work, Wallace modeled graphite as a two-dimensional (2D) quantum lattice, neglecting coupling to adjacent layers, and employed the tight-binding method. Starting from the Schrödinger equation, he derived an expression analogous to the Weyl–Dirac equation for massless fermions. The resulting band structure showed that the valence and conduction bands touch at a single point, from which a Dirac cone emerges. It was therefore concluded that 2D graphite behaves as a semimetal.

In 2005, Novoselov et al. experimentally validated Wallace's prediction by isolating single layers of carbon atoms, now known as graphene [2]. Subsequent studies [3,4] demonstrated graphene's extraordinary properties, which stem from its gapless band structure and Dirac cone-like energy dispersion—features characteristic of massless Dirac fermions and previously thought unattainable in a single-layer material. These findings have since established graphene as a central focus of condensed-matter research.

Other two-dimensional materials, including silicene and germanene, have also been investigated for their Dirac-like electronic behavior [5–7]. In these systems, the monolayer

geometry enhances phenomena such as a high surface-to-volume ratio, strong localization effects, and reduced screening perpendicular to the surface. Subsequent research has identified a broad range of monolayer materials, including gapless Dirac materials and those with non-zero parabolic bandgaps [8]. Among them, black phosphorus has emerged as a promising material for nonlinear optics due to its non-zero parabolic bandgap [9].

Lithium, a key material in battery technologies, has been extensively studied using tight-binding models and density functional theory [10–15]. As a highly reactive alkali metal with a body-centered cubic structure, it is the lightest solid element and contains only three electrons. Although monolayer alkali metals, including lithium, have been examined on various substrates to enhance device performance [8,16], a free-standing 2D lithium monolayer has not yet been reported. Here, we investigate a two-dimensional crystal as a theoretical approximation to a lithium monolayer using the Dirac equation.

2. Theory

In this section, we define a two-dimensional lithium lattice arranged in a square lattice and derive the matrix equation that determines its energy spectrum. We investigate a hypothetical lithium monolayer, consisting of a single atomic layer, hereafter referred to as 2D lithium. Regarding its shape, it is defined as a conventional square lattice. Figure 1 shows the portrait of the particles of the lithium atom in the lattice. The unit cell, outlined with the square in orange, contains one atom. The filled violet circles are the immobile nuclei at the lattice positions. The four first-nearest neighbors nuclei are denoted as 2, 3, 4, and 5, and the four second-nearest neighbors as 6, 7, 8, and 9, and so on. The pink circle determines which nuclei are the first-nearest neighbors. The green filled circles are the two internal electrons at their "instantaneous fictitious" positions. The pink filled circles correspond to the quasi-free electrons inside the 2D crystal. Further considerations on the system will be given in Section 3.

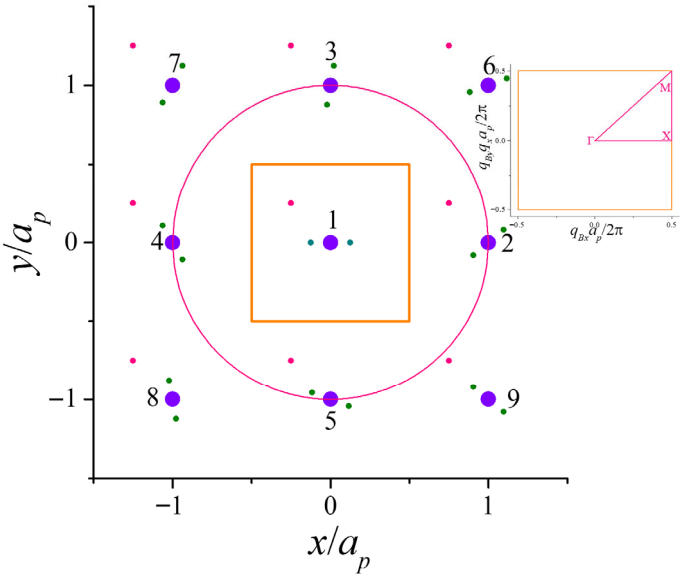


Figure 1. The square lattice and unit cell (orange) of the 2D lithium are shown. The filled violet circles correspond to the immobile nuclei, being the four nearest on the perimeter of the pink circle. The green filled circles are the electrons of the first orbital, and the pink filled circles are the third electron of the lithium atom. Inset: The first Brillouin Zone (BZ) (orange) and the irreducible BZ (pink). The high symmetry points are denoted by Γ, X and M.

The primitive lattice vectors correspond to those of a conventional square lattice, with $\vec{g}_1 = 2\pi/a_p\hat{i}$ and $\vec{g}_2 = 2\pi/a_p\hat{j}$ denoting the reciprocal lattice vectors.

In the electrostatic approximation, assuming immobile cores and a uniformly distributed electron density, the Dirac equation for an electron in a two-dimensional crystal is given by

$$\begin{bmatrix} +m_ec^2+V(x,y) & 0 & +cp_z & cp_x-icp_y \\ 0 & +m_ec^2+V(x,y) & cp_x+icp_y & -cp_z \\ cp_z & cp_x-icp_y & -m_ec^2+V(x,y) & 0 \\ cp_x+icp_y & -cp_z & 0 & -m_ec^2+V(x,y) \end{bmatrix} \times \begin{bmatrix} \psi_0\left(\vec{r},t\right) \\ \psi_1\left(\vec{r},t\right) \\ \psi_2\left(\vec{r},t\right) \\ \psi_3\left(\vec{r},t\right) \end{bmatrix} = i\hbar\frac{\partial}{\partial t}\begin{bmatrix} \psi_0\left(\vec{r},t\right) \\ \psi_1\left(\vec{r},t\right) \\ \psi_2\left(\vec{r},t\right) \\ \psi_3\left(\vec{r},t\right) \end{bmatrix}. \tag{1}$$

The interaction between the particles (nuclei and electrons) and the electron under study in the "central" cell, is depicted in the potential $V(x,y)$; see Appendix A and the beginning of Section 3 for further details.

Since the potential is periodic, it can be written as the Fourier expansion

$$V(x,y)=\sum_m\sum_n v_{m,n}\exp\left[i\left(\vec{g}_1m+\vec{g}_2n\right)\cdot\vec{r}\right], \tag{2}$$

where $\vec{g}_1=2\pi a_p^{-1}\hat{i}$ and $\vec{g}_2=2\pi a_p^{-1}\hat{j}$ are vectors of the reciprocal lattice.
The Bloch–Floquet theorem establishes that the solution to Equation (1) is

$$\vec{\psi}(x,y,t)=\sum_m\sum_n\vec{w}_{m,n}\exp\left[i\vec{q}_B\cdot\vec{r}+i\left(\vec{g}_1m+\vec{g}_2n\right)\cdot\vec{r}-iEt/\hbar\right], \tag{3}$$

where $\vec{w}_{m,n}$ is a four-component vector for each m, n, and $\vec{q}_B$ is the Bloch vector:

$$\vec{q}_B=q_{Bx}\hat{i}+q_{By}\hat{j}. \tag{4}$$

By using Equations (2) and (3) in (1), the following is obtained

$$\begin{aligned} \sum_{k,l}\begin{bmatrix} m_ec^2 & 0 & 0 & f_k^{(x)}-if_l^{(y)} \\ 0 & m_ec^2 & f_k^{(x)}+if_l^{(y)} & 0 \\ 0 & f_k^{(x)}-if_k^{(y)} & -m_ec^2 & 0 \\ f_k^{(x)}+if_l^{(y)} & 0 & 0 & -m_ec^2 \end{bmatrix}\begin{bmatrix} w_{k,l}^{(0)} \\ w_{k,l}^{(1)} \\ w_{k,l}^{(2)} \\ w_{k,l}^{(3)} \end{bmatrix} & \\ \times\exp\left[i\left(\vec{g}_1k+\vec{g}_2l\right)\cdot\vec{r}\right] & \\ +\sum_{k,k'}\sum_{l,l'}v_{k',l'}\begin{bmatrix} w_{k,l}^{(0)} \\ w_{k,l}^{(1)} \\ w_{k,l}^{(2)} \\ w_{k,l}^{(3)} \end{bmatrix}\exp\left[i\left(\vec{g}_1k'+\vec{g}_1k+\vec{g}_2l'+\vec{g}_2l\right)\cdot\vec{r}\right] & \\ =E\sum_{k,l}\begin{bmatrix} w_{k,l}^{(0)} \\ w_{k,l}^{(1)} \\ w_{k,l}^{(2)} \\ w_{k,l}^{(3)} \end{bmatrix}\exp\left[i\left(\vec{g}_1k+\vec{g}_2l\right)\cdot\vec{r}\right], & \end{aligned} \tag{5}$$

where

$$f_k^{(x)} = c\hbar\left(q_{Bx} + \frac{2\pi}{a_p}k\right) \tag{6}$$

and

$$f_l^{(y)} = c\hbar\left(q_{By} + \frac{2\pi}{a_p}l\right). \tag{7}$$

Multiplying Equation (5) by $\exp\left[-i\left(\vec{g}_1 m + \vec{g}_2 n\right)\cdot\vec{r}\right]$ and applying the orthogonality of the Fourier functions results in

$$\sum_{k,l}\begin{bmatrix} v_{m-k,n-l} + m_e c^2\delta_{k,m}\delta_{l,n} & 0 & 0 & \left(f_k^{(x)} - if_l^{(y)}\right)\delta_{k,m}\delta_{l,n} \\ 0 & v_{m-k,n-l} + m_e c^2\delta_{k,m}\delta_{l,n} & \left(f_k^{(x)} + if_l^{(y)}\right)\delta_{k,m}\delta_{l,n} & 0 \\ 0 & \left(f_k^{(x)} - if_l^{(y)}\right)\delta_{k,m}\delta_{l,n} & v_{m-k,n-l} - m_e c^2\delta_{k,m}\delta_{l,n} & 0 \\ \left(f_k^{(x)} + if_l^{(y)}\right)\delta_{k,m}\delta_{l,n} & 0 & 0 & v_{m-k,n-l} - m_e c^2\delta_{k,m}\delta_{l,n} \end{bmatrix}\begin{bmatrix} w_{k,l}^{(0)} \\ w_{k,l}^{(1)} \\ w_{k,l}^{(2)} \\ w_{k,l}^{(3)} \end{bmatrix} = E\begin{bmatrix} w_{m,n}^{(0)} \\ w_{m,n}^{(1)} \\ w_{m,n}^{(2)} \\ w_{m,n}^{(3)} \end{bmatrix}. \tag{8}$$

From an analysis of Equation (8), two matrix equations are found:

$$\sum_{k,l=-n_1}^{+n_1}\begin{bmatrix} v_{m-k,n-l} + m_e c^2\delta_{k,m}\delta_{l,n} & \left(f_{k,l}^{(x)} - if_{k,l}^{(y)}\right)\delta_{k,m}\delta_{l,n} \\ \left(f_{k,l}^{(x)} + if_{k,l}^{(y)}\right)\delta_{k,m}\delta_{l,n} & v_{m-k,n-l} - m_e c^2\delta_{k,m}\delta_{l,n} \end{bmatrix}\begin{bmatrix} w_{k,l}^{(0)} \\ w_{k,l}^{(3)} \end{bmatrix} = E\begin{bmatrix} w_{m,n}^{(0)} \\ w_{m,n}^{(3)} \end{bmatrix} \tag{9}$$

and

$$\sum_{k,l=-n_1}^{+n_1}\begin{bmatrix} v_{m-k,n-l} + m_e c^2\delta_{k,m}\delta_{l,n} & \left(f_{k,l}^{(x)} + if_{k,l}^{(y)}\right)\delta_{k,m}\delta_{l,n} \\ \left(f_{k,l}^{(x)} - if_{k,l}^{(y)}\right)\delta_{k,m}\delta_{l,n} & v_{m-k,n-l} - m_e c^2\delta_{k,m}\delta_{l,n} \end{bmatrix}\begin{bmatrix} w_{k,l}^{(1)} \\ w_{k,l}^{(2)} \end{bmatrix} = E\begin{bmatrix} w_{m,n}^{(1)} \\ w_{m,n}^{(2)} \end{bmatrix}. \tag{10}$$

This means that the system is two-fold degenerated. Equations (9) or (10) provide two sets of energies associated with the electrons and positrons.

In the next section, Equation (10) will be solved numerically to study the dependence of the energies on several parameters of the system.

The density of probability is calculated according to the expression

$$\left|\vec{\psi}(x,y,t)\right|^2 = \sum_{m,k}\sum_{n,l}\left[w_{m,n}^{(1)*}w_{k,l}^{(1)} + w_{m,n}^{(2)*}w_{k,l}^{(2)}\right] \times\exp\left\{i2\pi a_p^{-1}[(m-k)x + (n-l)y]\right\}. \tag{11}$$

3. Numerical Results

In this section, the energies, as a function of n_1, l_{pa} and n_c, parameters related to the dimension of the eigenvalue equation, the partition of the potential of the unit cell, and the number of neighboring cells that affect the electron, respectively, are studied. Now we will focus on the electronic transport properties of 2D lithium.

To solve this problem, the electrostatic approximation is used. The first assumption is that the nuclei occupy fixed positions at the lattice sites. In the unit cell labeled as "1" in Figure 1, the electron in the external orbit is the object of study, and it is considered that the two inner electrons are strongly bounded to the nucleus and taken as a circular charge distribution at the Bohr radius for the lithium atom. In neighboring cells, the two electrons in the first orbit are assumed to form, together with the nucleus, a positive ion with a net

charge of +e that generates a negative potential. The outer quasi-free electron is assumed to be uniformly distributed across the unit cell maintaining the fourfold symmetry of the lattice. The electron of study is likely to be in any point of the unit cell (except at the center and at the Bohr radius), and the potential that defines the lattice is calculated considering the Coulomb interaction between this electron and the particles that surround it. If the electron were at the center of the cell or at the Bohr radius, the potential would be infinite in magnitude given its proportionality with $1/r$, where r is the distance between the charges. No further considerations are assumed, and the period of the lattice is that of solid lithium: $a_p = 3.5$ Å.

Convergence was tested for the parameters n_1, n_c and l_{pa}, in the following calculations, only one of which is varied while the others remain fixed. When a parameter is increased, computation time increases too. Each parameter has its own convergence due to computing power.

3.1. Convergence of the Energies

In this section, we analyze how the energies converge as function n_1, the dimension of the truncated matrix of Equation (10). Higher values of n_1 lead to larger matrix dimensions, which enhance the convergence of the results. However, this also increases the computational time and memory requirements.

In Figure 2, the five most negative energies at points (a) M, (b) X and (c) Γ are shown as a function of n_1. The matrix dimension is $n_{dim} = 2(2n_1 + 1)^2$. Of course, other values of the wave vector can also be chosen. For computational restrictions, the best convergence achieved for the deepest band was $\Delta E_{n_1} = 0.91$ at point M, where $\Delta E_{n_1} = E_{n_1} - E_{n_1-1}$ with $n_1 = 17, 18, \ldots, 37$. The red-colored band corresponds to the left axis. The bands that correspond to the right axis, from more to less negative, are the blue, the magenta, the dark yellow and the navy-colored bands. The scales with the arrow indicate the bands with the corresponding colors: blue (E_{D2}), magenta (E_{D3}), dark yellow (E_{D4}) and navy (E_{D5}). The case is similar for the following figures. The blue-colored energies overlap with the magenta-colored ones. The most negative energy (red-colored) shows an exponentially decaying behavior. A similar case, but on a much lower scale, is for the dark yellow-colored energies. The other energies are almost independent of this parameter n_1.

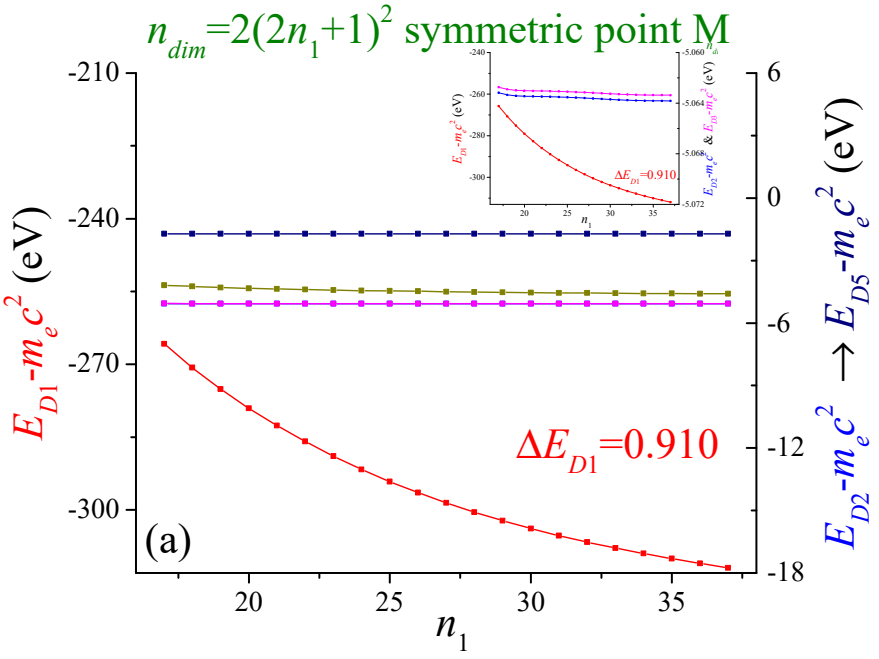


Figure 2. *Cont.*

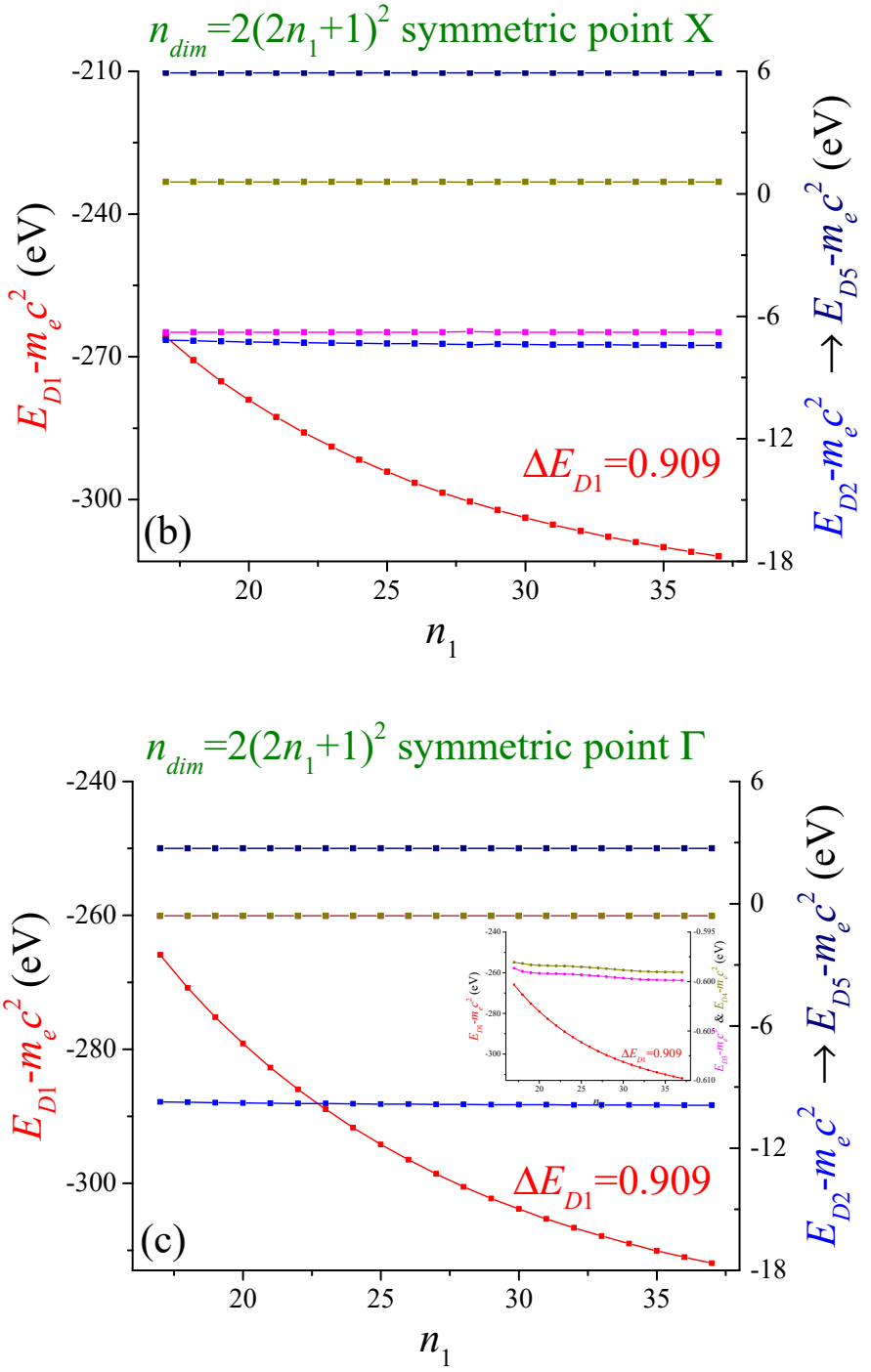


Figure 2. The energies of the five most negative of the two-dimensional lithium at the high symmetry points (**a**) M, (**b**) X and (**c**) Γ are shown as function n_1. The lattice period is $a_p = 0.35$ nm. The square unit cell is divided in l_{pa} times l_{pa} pieces, with $l_{pa} = 2048$. The number of cells that affect the electron are $n_c = 393$.

The bands show different convergence behavior as n_1 is increased. The red color band is the most dependent on this parameter. The bands related to the right axis achieved good convergence. For the sake of our calculations, the convergence criterion was set with $n_1 = 37$.

3.2. The Atoms That Affect the Electron

The electron of study is affected by the particles in the first unit cell and the ones in neighboring atoms. The interaction between these particles and the electron is of a

Coulomb type and the potential in the unit cell is calculated accordingly. This section studies the influence of the atoms that surround the electron on its energies in function of the parameter n_c.

In Figure 3, the five most negative energies and the least positive energy, at point M, are shown as a function of n_c, with $n_1 = 16$ ($n_{dim} = 2178$), and $l_{pa} = 8192$. Here, $\Delta E_{n_c} = E_{n_c} - E_{n_c-8}$ with $n_c = 161, 169, \ldots, 261$. The blue-colored energies overlap with the magenta-colored ones. The parameter n_C is the number of atoms (nucleus and electrons) selected to influence the electron in the central cell. Theoretically, in a real crystal, this number should approach infinity. Our calculations suggest that $n_c = 161$ atoms surrounding the central cell are enough to account for the contribution to the potential in the central cell. The convergence achieved for the deepest band was $\Delta E_{n_c} = 0.0008$ eV. In the inset, the difference ΔE_{n_c} for the most negative energy (violet-colored) is shown. All bands showed good convergence.

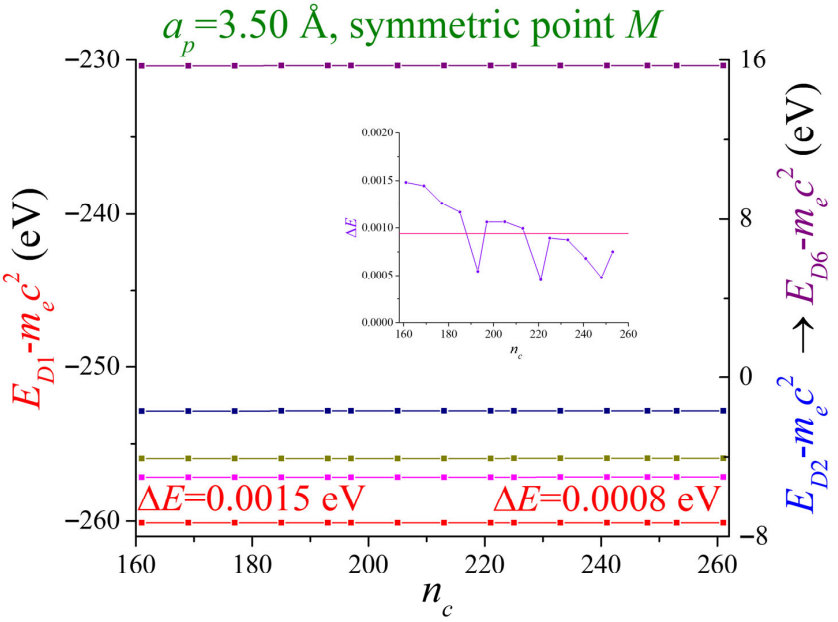


Figure 3. The energies of two-dimensional lithium at the high symmetry point M are shown as a function n_c. A number of 261 nearest neighbor atoms are selected to perform this calculation obtaining the value $\Delta E_{n_c} = 0.0008$ eV for the most negative energy. In the other high symmetry points this behavior is also observed. The lattice period is $a_p = 0.35$ nm. The lattice is divided with the factor $l_{pa} = 8192$. The parameter related to the matrix dimension is $n_1 = 16$.

For the range of values of n_c, the energy bands shown in Figure 3 display small dependence on the increment of n_c. Although the dependence of the energy value is minimal in the range shown in Figure 3, the value of $n_c = 393$ was chosen because it is the highest value allowed computationally.

3.3. The Partition of the Unit Cell

The potential that defines the crystal for the electron of study required for Equation (10) is calculated with a numerical method dividing the unit cell into a $l_{pa} \times l_{pa}$ number of small square sections where it is assumed that the potential is constant. The larger the number l_{pa} is, the smaller the sections of the unit cell are, thus making the potential more accurate. Then, the Fourier coefficients of the potential are calculated. In this section, the behavior of the energies is studied in function of the parameter l_{pa}. The procedure of the calculation of the coefficients of the potential is presented in Appendix A.

In Figure 4, the five most negative energies at the symmetric point M are shown as a function of l_{pa}. Here, $\Delta E_{l_{pa}} = E_{l_{pa}=2^n} - E_{l_{pa=2^{n-1}}}$ with $l_{pa} = 1024, 2048, 4096, 8192$.

The matrix dimension is given by $n_1 = 23$ ($n_{dim} = 4418$). The l_{pa} parameter is related to the number of pieces ($l_{pa} \times l_{pa}$) in which the unit cell is divided to obtain the Fourier coefficients of the potential. The number of atoms that affect the electron is $n_c = 393$. The overall energies show a stable behavior with this parameter; only the most negative shows an exponential decay behavior. The convergence achieved for the red-colored band was $\Delta E = 1.6$ eV. The bands related to the right axis achieved good convergence.

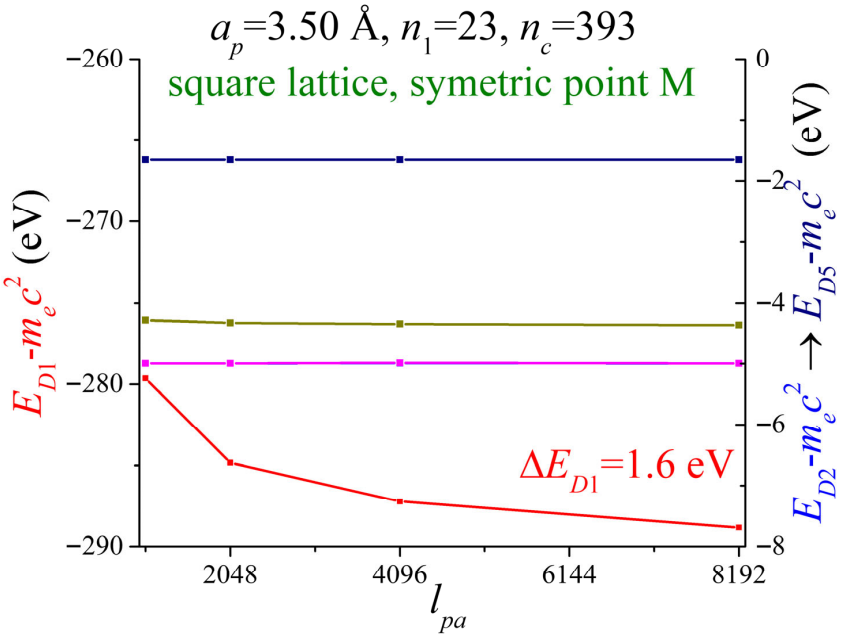


Figure 4. The energies of two-dimensional lithium at the high symmetry point M are shown as a function of l_{pa}. The lattice period is $a_p = 0.35$ nm. The number of atoms that affect the electron are $n_c = 393$. The parameter related to the matrix dimension is $n_1 = 23$.

The red-colored band exhibits a stronger dependence on the parameter l_{pa}. Due to computation restrictions, we stop at $l_{pa} = 8192$.

So far, this section has examined how the energies vary with the three main parameters n_1, n_c and l_{pa}. The energy of the most negative state showed more sensitivity on n_1 and l_{pa} than the other energies. Thus, the remaining energies are less dependent on the three parameters.

3.4. The Band Structure of 2D Lithium

Having studied convergence in the energies varying the main parameters related to the dimension of the eigenvalue matrix equation, the number of atoms that affect the electron in the central cell, and the number of partitions of the unit cell to calculate the Fourier coefficients of the potential, the next step is to calculate the band structure of 2D lithium.

Figure 5 shows the band structure of 2D lithium for an electron in the central cell. The parameters used are $n_1 = 37$, $l_{pa} = 8192$, and $n_c = 393$. The period of the lattice is $a_p = 0.35$ nm. The interaction between the electron and the particles in the central cell and the ones in neighboring atoms is of the Coulomb (electrostatic) type. The convergence for the red-colored band is $\Delta E = 0.9$ eV. The bands related to the right axis achieved good convergence. The red-colored energies related to the left axis show small dependence on the propagation wave vector and its magnitude is very large. As can be seen in Figure 4, only the deepest band shows a strong dependence on the l_{pa} parameter. According to our definition for the potential, when the l_{pa} parameter increases, the potential magnitude near the nucleus also increases, and the energy of this band decreases. Further study is needed to determine whether more restrictions should be applied to the possible locations of the

electron under study. Based on the information in Figure 4, we expect that the other bands will not undergo significant changes. The values of the lowest band have an energetic variation about 0.1 eV, being an almost flat band. A complete band gap appears between the red- and the blue-colored energy band. It is also possible, although unlikely, that the red-colored band corresponds to spurious solutions of the eigenvalue equation, meaning that this band does not have a physical interpretation. The bands related to the right axis represent anisotropy in 2D lithium and show no complete band gap. The blue-, magenta-, and dark yellow-colored bands show from quasi-free (mostly in the middle between high symmetry points) to quasi-bound (mostly on the high symmetry points) behavior for the electron. If the Fermi level is considered to be at 0 eV, the dark yellow- and the navy-colored bands corroborate the metallic behavior that would be expected from the uniform electron gas type model that we applied in the definition of the potential.

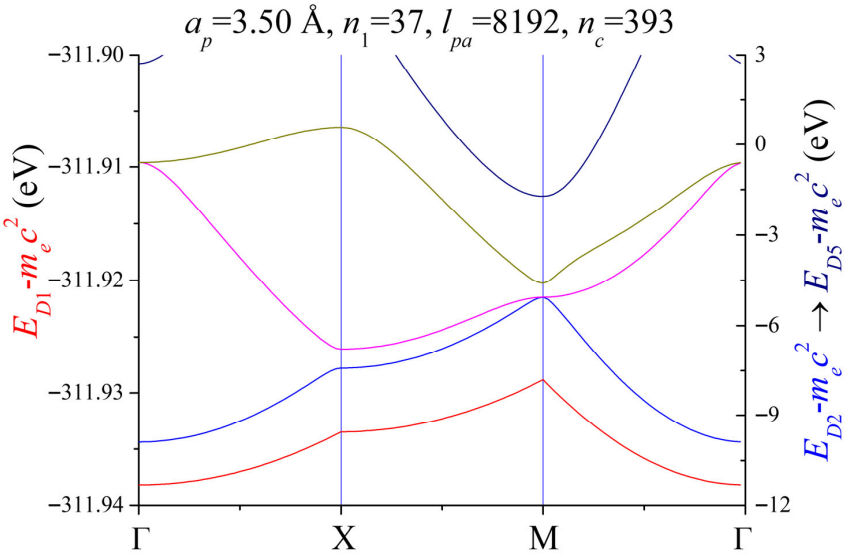


Figure 5. Electronic band structure of 2D lithium. The high symmetry directions are marked in the horizontal axis. The lattice period is $a_p = 0.35$ nm. The number of atoms that affect the electron are $n_c = 393$. The parameter related to the matrix dimension is $n_1 = 37$.

4. Conclusions

The energy bands of two-dimensional lithium were computed by applying the plane-wave expansion to the Dirac equation. The convergence of the energies was examined in terms of the parameters defining the physical and mathematical model: the dimension of the eigenvalue matrix (n_1), the number of atoms that affect the electron in the central cell considering an electrostatic Coulomb interaction (n_c), and the partition of the unit cell given by l_{pa} in the calculation of the potential. The period a_p of the lattice was fixed to 0.35 nm, in concordance with solid lithium. In the band structure, the convergence criterion was good except for the most negative band. The behavior of the electron was discussed for the remaining bands, which showed different properties for 2D lithium, including metallic behavior which is consistent with the definition of the potential in the lattice.

Author Contributions: Conceptualization, R.A.M.-S.; methodology, R.G.-L.; software, R.G.-L. and J.A.G.-A.; validation, J.A.G.-A. and R.A.M.-S.; formal analysis, J.D.V.-S. and J.A.G.-A.; investigation, J.D.V.-S.; resources, J.A.G.-A.; data curation, R.G.-L.; writing—original draft preparation, R.G.-L. and J.D.V.-S.; writing—review and editing, J.D.V.-S. and R.A.M.-S.; visualization, R.G.-L.; supervision, R.A.M.-S.; project administration, R.G.-L. All authors have read and agreed to the published version of the manuscript.

Funding: R.A.M.-S. was supported by DGAPA-UNAM under project IN118825. Financial support from CONAHCYT under Grant No. CF-2023-G-763 is acknowledged.

Data Availability Statement: The raw data supporting the conclusions of this article will be made available by the authors on reasonable request.

Acknowledgments: The authors thank the High-Performance Computing Area of the Universidad de Sonora (ACARUS) for the use of its supercomputing infrastructure, which was fundamental to the development of this work.

Conflicts of Interest: The authors declare no conflicts of interest.

Abbreviations

The following abbreviations are used in this manuscript:

2D	two-dimensional
DFT	density functional theory
BCC	body-centered cubic
BZ	Brillouin Zone

Appendix A. Fourier's Coefficients of the Potential

The Fourier's coefficients of the potential of a 2D crystal are given by

$$v_{m,n} = \frac{1}{\left|\vec{a}_1 \times \vec{a}_2\right|}\int_{cu} V(x,y)\exp\left[-i\left(\vec{g}_1 m + \vec{g}_2 n\right)\cdot\vec{r}\right]da. \tag{A1}$$

Considering our system, the coefficients become

$$v_{m,n} = -\frac{q_e^2}{4\pi\varepsilon_0}\frac{1}{a_p^2}\int_{-\frac{ap}{2}}^{+\frac{ap}{2}}\int_{-\frac{ap}{2}}^{+\frac{ap}{2}} dx'dy'V(x',y')\exp\left(-ig_p m x' - ig_p n y'\right). \tag{A2}$$

Defining $x_k = -0.5 + 0.5(2l-1)\Delta x$ and $y_l = -0.5 + 0.5(2l-1)\Delta y$, and assuming that the potential, shown explicitly in Equation (A3), is constant in the integrals, we obtain

$$\begin{aligned}
&v_{m,n}\\
&= -\frac{q_e^2}{4\pi\varepsilon_0 a_p}\sum_{k=1}^{l_{pa}}\sum_{l=1}^{l_{pa}}\Bigg\{\frac{Z}{\sqrt{\left(x_k^{(r)}\right)^2+\left(y_l^{(r)}\right)^2}}\\
&-\sum_{m=1}^{m_{e1}}\frac{1}{\sqrt{\left[x_k^{(r)}-r_{bn}\cos\theta_{em}\right]^2+\left[y_l^{(r)}-r_{bn}\sin\theta_{em}\right]^2}}\\
&-\sum_{m=1}^{m_{e2}}\frac{1}{\sqrt{\left[x_k^{(r)}+r_{bn}\cos\theta_{em}\right]^2+\left[y_l^{(r)}+r_{bn}\sin\theta_{em}\right]^2}}\\
&+\sum_{o=2}^{n_c}\Bigg[\frac{1}{\sqrt{\left(x_k^{(r)}-x_o^{(n)}\right)^2+\left(y_l^{(r)}-y_o^{(n)}\right)^2}}\\
&-\sum_{m=1}^{m_{e3}}\frac{1}{\sqrt{\left[x_k^{(r)}-\left(x_o^{(n)}-R_{bm}\cos\theta_{Rm}\right)\right]^2+\left[y_l^{(r)}-\left(y_o^{(n)}-R_{bm}\sin\theta_{Rm}\right)\right]^2}}\Bigg]\Bigg\}\\
&\times\int_{x_k-\Delta x/2}^{x_k-\Delta x/2}dx\,\exp\left(-ig_p a_p m x\right)\int_{y_l-\Delta x/2}^{y_l-\Delta x/2}dy\,\exp\left(-ig_p a_p n y\right),
\end{aligned} \tag{A3}$$

where r_{bn} is the ratio between the Bohr radius r_b of the internal electrons and the period a_p; n_c is the number of cores that affect the electron; and R_{bm} is the ratio between the Bohr radius R_b of the external electron. In this series n_c tends to infinitum.

Integrating Equation (A3), the expression for the coefficients is

$$v_{m,n} = \frac{\sin(m\pi\Delta x)}{m\pi}\frac{\sin(n\pi\Delta y)}{n\pi}\sum_{k=1}^{l_{pa}}\sum_{l=1}^{l_{pa}} V(x_k, y_k)\exp(-i2\pi m x_k)\exp(-i2\pi n y_k). \quad \text{(A4)}$$

References

1. Wallace, P.R. The band theory of graphite. *Phys. Rev.* **1947**, *71*, 622–634. [CrossRef]
2. Novoselov, K.S.; Jiang, D.; Schedin, F.; Geim, A.K. Two-dimensional atomic crystals. *Proc. Natl. Acad. Sci. USA* **2005**, *102*, 10451–10453. [CrossRef]
3. Novoselov, K.S.; Geim, A.K.; Morozov, S.V.; Jiang, D.; Zhang, Y.; Dubonos, S.V.; Grigorieva, I.V.; Firsov, A.A. Electric Field Effect in Atomically Thin Carbon Films. *Science* **2004**, *306*, 666–669. [CrossRef] [PubMed]
4. Novoselov, K.S.; Geim, A.K.; Morozov, S.V.; Jiang, D.; Katsnelson, M.I.; Grigorieva, I.V.; Dubonos, S.V.; Firsov, A.A. Two-dimensional gas of massless Dirac fermions in graphene. *Nature* **2005**, *438*, 197–200. [CrossRef]
5. Şahin, H.; Cahangirov, S.; Topsakal, M.; Bekaroglu, E.; Akturk, E.; Senger, R.T.; Ciraci, S. Monolayer honeycomb structures of group-IV elements and III-V binary compounds: First-principles calculations. *Phys. Rev. B* **2009**, *80*, 155453. [CrossRef]
6. Cahangirov, S.; Topsakal, M.; Aktürk, E.; Şahin, H.; Ciraci, S. Two- and One-Dimensional Honeycomb Structures of Silicon and Germanium. *Phys. Rev. Lett.* **2009**, *102*, 236804. [CrossRef]
7. Fleurence, A.; Friedlein, R.; Ozaki, T.; Kawai, H.; Wang, Y.; Yamada-Takamura, Y. Experimental Evidence for Epitaxial Silicene on Diboride Thin Films. *Phys. Rev. Lett.* **2012**, *108*, 245501. [CrossRef]
8. Liu, G.; Cui, Z.; Zhang, F.; Zeng, Y.; Chen, W.; Liu, Y.; Nie, Z.; Bao, Q. Emerging 2D Materials with Nonparabolic Bands for Ultrafast Photonics. *Small Sci.* **2023**, *3*, 2300030. [CrossRef] [PubMed]
9. Chen, X.; Ponraj, J.S.; Fan, D.; Zhang, H. An overview of the optical properties and applications of black phosphorus. *Nanoscale* **2020**, *12*, 3513–3534. [CrossRef] [PubMed]
10. Callaway, J.; Zou, X.; Bagayoko, D. Total energy of metallic lithium. *Phys. Rev. B* **1983**, *27*, 631–635. [CrossRef]
11. Popov, V.A. Electronic band structure of metallic lithium in the field of external excitation. *Comp. Mat. Sci.* **1999**, *14*, 67–71. [CrossRef]
12. Gao, R.; Hu, Z.; Mao, J.; Chen, S.; Yam, C.Y.; Chen, G.H. Self-Consistent-Charge Density-Functional Tight-Binding Parameters for Modeling an All-Solid-State Lithium Battery. *J. Chem. Theory Comput.* **2023**, *19*, 1381–1387. [CrossRef] [PubMed]
13. Oviedo, M.B.; Fernandez, F.; Otero, M.; Leiva, E.P.M.; Paz, S.A. Density Functional Tight-Binding Model for Lithium–Silicon Alloys. *J. Phys. Chem. A* **2023**, *127*, 2637–2645. [CrossRef] [PubMed]
14. Chaney, R.C.; Lafon, E.E.; Lin, C.C. Energy Band Structure of Lithium Fluoride Crystals by the Method of Tight Binding. *Phys. Rev. B* **1971**, *4*, 2734–2741. [CrossRef]
15. Lafon, E.E.; Lin, C.C. Energy band structure of lithium by the tight-binding method. *Phys. Rev.* **1966**, *152*, 579–584. [CrossRef]
16. Farjam, M.; Rafii-Tabar, H. Energy gap opening in submonolayer lithium on graphene: Local density functional and tight-binding calculations. *Phys. Rev. B* **2009**, *79*, 045417. [CrossRef]

Disclaimer/Publisher's Note: The statements, opinions and data contained in all publications are solely those of the individual author(s) and contributor(s) and not of MDPI and/or the editor(s). MDPI and/or the editor(s) disclaim responsibility for any injury to people or property resulting from any ideas, methods, instructions or products referred to in the content.